# ANALYTICAL AND EXPERIMENTAL STUDIES ON CREEP BEHAVIOR OF POLYMERIC MATRIX COMPOSITES

K. Y. Lin* and I. H. Hwang†

*Department of Aeronautics and Astronautics*
*University of Washington*
*Seattle, Washington 98195, U.S.A.*

## Abstract

The creep behavior of graphite/epoxy composites is studied both analytically and experimentally. In the analytical study, a special finite element procedure was developed for the accurate and efficient analysis of creep response in anisotropic materials. This procedure was used to study the stress and strain distributions and histories in composite laminates containing circular holes. In the experimental study, creep tests were performed to investigate the time-dependent response of graphite/epoxy composites at elevated temperature. The moiré interferometry technique was employed to determine the deformation histories in notched composites. The experimental results were compared with the analytical predictions and good agreement was observed.

## Introduction

Advanced composite materials, especially graphite/epoxy, have been widely applied to airplane structures, and the trend is rapidly increasing. Composite materials possess advantages over the conventional metallic materials when the stiffness and strength are taken into account on a unit weight basis. Composites also offer an improvement in resistance to fatigue failure and resistance to corrosion. These superior properties lead to a new airplane design phase where high performance and energy saving can be effectively achieved.

An important consideration in composite design is the durability of a structure in the presence of thermal and moisture environments over a long time period. When a composite is exposed to hygrothermal environments, problems of dimensional stability, residual stress, and material degradation can occur. Depending on the specific load spectrum, the induced residual stress can be sufficiently large to cause microcracking in the matrix. This is particularly important for structures with geometric discontinuities in which the failure can initiate near the stress concentration site. This type of problem can not be fully described by a static elastic analysis since the material properties degrade with time. Several investigators have suggested employing the viscoelastic theory to account for such time-dependent effects in composites [1-6].

The studies of viscoelastic effects in composites have been mainly limited either to material characterization tests or to the analysis of simple problems which can be solved by incremental classical lamination theory. In the present study, the creep behavior of graphite/epoxy composites is investigated both analytically and experimentally. In the analytical study, a special finite element procedure was developed for the accurate and efficient analysis of thermoviscoelastic boundary value problems in composites [7]. The integral form of viscoelastic constitutive relations was used and the resulting finite element equilibrium equations were solved using the recursive formula. The developed analysis procedure was used to study the stress and strain distributions and histories in composite laminates containing circular holes.

In the experimental study, an experimental program was designed to verify the analytical results. Although some experimental studies have been performed to characterize viscoelastic material properties, there has been no attempt to measure full-field creep deformation of composite materials at elevated temperatures. Application of high frequency moiré interferometry to composite materials for the measurement of time-dependent in-plane deformations was explored. The creep test was conducted at 121°C/dry which represents a typical environment for commercial airplane operations. The time-dependent deformations around a circular hole in composites were measured and compared with the numerical predictions.

## Finite Element Formulation

The linear viscoelastic constitutive equations can be expressed in the integral form using the contracted notations for stresses ($\sigma_i$), strains ($\varepsilon_i$), and relaxation moduli ($Q_{ij}$) as follows

$$\sigma_i(t) = \int_{-\infty}^{t} Q_{ij}(T, t - \tau) \frac{\partial \varepsilon_j(\tau)}{\partial \tau} d\tau \tag{1}$$

where the relaxation moduli $Q_{ij}$ are functions of temperature (T) and time (t). Using the time temperature

---

* Associate Professor, † Graduate Research Assistant.

superposition principle the relaxation function can be obtained from the master curve:

$$Q_{ij}(T, t) = Q_{ij}(T_o, \zeta_{ij}(t)) \qquad (2)$$

where $T_o$ is the reference temperature and $\zeta_{ij}$ is the reduced time. The four relaxation functions in the principal material directions are expanded into the exponential series.

$$Q_{ij}(t) = Q_{ij,0} + \sum_{\omega=1}^{N} Q_{ij,\omega} \exp(-t/\lambda_{ij,\omega}) \qquad (3)$$

where $\lambda_{ij,\omega}$ is the relaxation time obtained from each master curve. The moduli $\overline{Q}_{ij}$ along the natural body axes (xy) can be obtained from the tensor transformation.

In the finite element development two-dimensional quadrilateral elements were formulated using the isoparametric mapping. The displacements within an element were interpolated in terms of nodal displacements. Using the variational theorem the element equilibrium equation was derived. Element stiffness matrices and force vectors were assembled to yield the global equations:

$$K_{mn}(\zeta) \, u_n(0) + \int_0^t K_{mn}(\zeta - \zeta') \frac{\partial u_n}{\partial \tau} d\tau = F_m(t) \qquad (4)$$

where m, n = 1, 2, 3, ..., number of degrees of freedom. $K_{mn}$ is the stiffness matrix, $u_n$ is the nodal displacement, and $F_m$ is the force vector due to the prescribed tractions. A recursive numerical scheme developed by Lin and Hwang [7] was used to solve the integral equation (4).

## Experimental Procedure

The creep test was conducted at 121°C and dry condition. This temperature was achieved using an air-circulating oven. A custom-made creep load frame was used in the test. Combinations of several dead weights were used to apply constant loads. The IM7/8551-7 graphite/epoxy composite was chosen in the test. The composite specimen was 2.54 cm wide by 25.4 cm long. The notched specimen had a circular hole of 0.635 cm diameter at the center (Figure 1a). The MM WK-series strain gauges with an electric resistance of 350 Ω were used for elevated temperature tests.

In the moiré interferometry tests, a 35 mw helium-neon laser with a wavelength of 632.8 nm was used as the light source. A system of mirrors was used to direct two collimated beams with the opposite incident angles to the specimen [8]. The crossed-line grating used in this study has the frequency, $F_s$, of 600 lines/mm in both directions. 600 Å aluminum coating was vacuum deposited on the holographic plate with diffraction gratings.

Material characterization tests were first performed to determine the viscoelastic properties and the results were used in the finite element analysis. A unidirectional $(0)_{12}$ laminate was tested to obtain the compliance $S_{11}$. The $S_{11}$ value was found to be time-independent at 121°C. The Poisson's ratio $\nu_{12}$ was assumed to be time-independent. The material properties were determined as:

$$E_{11} = 137.9 \text{ GPa}, \quad \nu_{12} = 0.34$$

In order to obtain the time-dependent compliance $S_{22}$, the $(90)_{24}$ laminate was loaded to 12.53 MPa and tested at 121°C for 48 hours. The instantaneous compliance $S_{22}(0)$ at 121°C was found to be 0.137 (1/GPa). Utilizing both the Prony technique and the least square method, the exponential series of the time-dependent creep compliance, $S_{22}(t)$, was computed from these test data as follows:

$$S_{22}(t) = S_{22}(0) \, g(t)$$
$$= S_{22}(0) \left\{ g_0 - \sum_{i=1}^{N} g_i \exp(-t/\lambda_i) \right\} \qquad (5)$$

where g(t) is a normalized function, i.e., g(0) = 1. The values of the coefficients $g_i$ are shown in Table 1.

The shear compliance $S_{66}$ was determined from the test data of a $(45/-45)_{3s}$ laminate. T-type strain gages were mounted to measure the strain components in both loading and transverse directions. Creep strains of the $(45/-45)_{3s}$ laminate were measured to 72 hours at 121°C under a stress of 34.47 MPa. The instantaneous shear compliance $S_{66}(0)$ was determined as 0.258 (1/GPa). The time function of the in-plane shear compliance, $S_{66}$, was calculated from the measured normal strains in the $(\pm 45)$, laminate [9].

The shear compliance, $S_{66}(t)$, has the same exponential series form as the transverse compliance, $S_{22}(t)$ in Eq. (5). The coefficients of the series are given in Table 2.

For a linear viscoelastic material there is a relation between the relaxation moduli and the creep compliances which can be derived from the stress-strain relations.

$$\int_0^t Q_{ij}(\tau) \, S_{jk}(t - \tau) \, d\tau = t \, \delta_{ik} \qquad (6)$$

Using the exponential series of the compliance in Eq. (5), the above integral equation can be solved numerically to determine the relaxation moduli [9]. Results for the coefficients of the relaxation moduli, $Q_{22}(t)$ and $Q_{66}(t)$, are presented in Table 1 and Table 2, respectively.

## Experimental Results

Creep tests on the $(90_2/\pm45/90/\pm45/90)_s$ specimen were conducted for 48 hours at the temperature of 121°C. The applied stress was 24.33 MPa. The resulting moiré fringes for the $u_x$ displacements are shown and compared with the finite element solutions in Figure 2 for t=1 minute and in Figure 3 for t=48 hours. The finite element solutions were obtained using the viscoelastic material properties from the creep tests of the unnotched composites. The contour plots were generated in such a way that the difference of the $u_x$ values between an iso-displacement line and the neighboring lines was equal to $8.333 \times 10^{-4}$ mm. This value can be calculated from $1/(2F_s)$ which represents the difference of $u_x$ between two neighboring lines. The overall fringe pattern of this laminate was similar to those found in an isotropic panel [10]. Note that the fringe densities are much higher near the hole edge. The maximum density was located at the hole edge near $\phi = 90°$ and 270°, indicating strain (or stress) concentration in this region. The minimum density occured in the directions of $\phi = 0°$ and $\phi = 180°$.

The distributions of the $u_x$-displacement along the hole edge (r = a) are shown for both t = 1 minute and t = 48 hours in Figure 4. Good agreement is observed between the experiment and the analysis in both cases. At t = 1 minute, the finite element solutions for the $u_x$ displacements ($\phi = 0°$ and $\phi = 180°$) are within 5% of the data measured by the moire interferometry.

The time response of the $u_x$ displacement was studied from several photographs at different creep times. The normalized displacement history at the point of $\phi = 0°$ and r = a is shown in Figure 5 for a period of two days. Shown in the same figure are the predictions from the finite element analysis. Again, good agreement between these two results is observed. Specifically, the moiré test measured a 19% increase in $u_x$ values after 48 hours while the finite element solution predicted a 17% increase for the same period.

The strain gages were also used to measure the creep and recovery strains in the $(90_2/\pm45/90/\pm45/90)_s$ laminate. A recovery time of 4 hours was selected. The creep strains measured by the strain gages and moire interferometry are compared with the finite element predictions in Figure 6. After 48 hours of creep, the strain gages recorded 21% and 18% increases at gage locations #1 and #2, respectively. Both the numerical solution and the moiré data were taken at location #1. The finite element analysis predicted a 22% increase, while a 25% increase was obtained from the moiré test. Upon unloading, strains dropped instantaneously. The instantaneous changes were about the same as the initial strains due to loading, which is a characteristic of linear viscoelasticity. During the recovery after unloading the test data deviate from the predictions. The experimental data shows a slower rate of recovery than the analysis.

## Conclusions

Analytical and experimental studies were carried out to investigate the creep response of polymeric matrix composites at elevated temperature. A special finite element procedure was developed for the efficient analysis of creep strain histories in composite structures with complex geometry. Numerical results were presented to illustrate the significance of creep response in polymeric composites. In the experiment, the moiré interferometry technique was employed to determine the time-dependent deformations of composites at elevated temperature. The measured displacement fields were compared with the finite element solutions. The strain histories measured by the moire interferometry and strain gages show fairly good agreement with the predictions by the finite element analysis. In addition, the instantaneous strain changes due to loading and unloading were found to be about the same, indicating that the response of the laminates studied was linearly viscoelastic.

## Acknowledgement

## References

1.  Sims, D.E., and Halpin, J.C., "Methods of Determining the Elastic and Viscoelastic Response of Composite Materials," ASTM STP 546, 1974, p. 46.

2.  Crossman, F.W., Mauri, R.E., and Warren, W.J., "Moisture-Altered Viscoelastic Response of Graphite/Epoxy Composites," ASTM STP 658, 1978, p.205.

3.  Yeow, Y.T., Morris, D.H., and Brinson, H.F., "Time-Temperature Behavior of a Unidirectional Graphite/Epoxy Composite," ASTM STP 674, 1979, p. 263.

4.  Flaggs, D.L., and Crossman, F.W., "Analysis of the Viscoelastic Response of Composite Laminates During Hygrothermal Exposure," J. of Composite Materials, Vol. 15, Jan. 1981, p. 21.

5.  Harper, B.D., and Weitsman, Y., "On the Effects of Environmental Conditioning on Residual Stresses in Composite Laminates," Int. J. of Solids & Structures, Vol. 21, 1985, p. 907.

6.  Tuttle, M.E., and Brinson, H.F., "Prediction of the Long-Term Creep Compliance of General Composite Laminates," Experimental Mechanics, Vol. 26 (1), March 1986, p. 89

7. Lin, K.Y. and Hwang, I.H., "Thermo-Viscoelastic Analysis of Composite Materials," J. of Composite Materials, Vol. 23, 1989, p. 535.

8. Post, D., "Moiré Interferometry," Handbook on Experimental Mechanics, Prentice-Hall, New Jersey, 1987, p. 314.

9. Hwang, I.H., "Thermo-Viscoelastic Behavior of Composite Materials," Ph.D. Dissertation, Department of Aeronautics and Astronautics, University of Washington, 1990.

10. Lauler, L.T., "Effect of Diffraction Grating Thickness in Moiré Interferometry," M.S. Thesis, Department of Aeronautics and Astronautics, University of Washington, 1988.

**Table 2** Coefficients for the normalized shear compliance $S_{66}$ and modulus $Q_{66}$

$$S_{66}(t)/S_{66}(0) = g_o - \sum_{i=1}^{N} g_i \exp\left(- t/\lambda_i\right)$$

$$Q_{66}(t)/Q_{66}(0) = f_o + \sum_{i=1}^{N} f_i \exp\left(- t/\lambda_i\right)$$

| i | $g_i$ | $f_i$ | $\lambda_i$ |
|---|-------|-------|-------------|
| 0 | 2.61726 | 0.38208 | |
| 1 | 0.13995 | 0.02102 | $2.5920 \times 10^5$ |
| 2 | 0.27354 | 0.01241 | $4.0913 \times 10^4$ |
| 3 | 0.76258 | 0.18082 | $1.2479 \times 10^4$ |
| 4 | 0.18079 | 0.21157 | $2.1913 \times 10^3$ |
| 5 | 0.14269 | 0.0691 | $5.782 \times 10^2$ |
| 6 | 0.11771 | 0.1230 | $6.000 \times 10^1$ |

**Table 1** Coefficients $g_i$ and $f_i$ for the normalized transverse compliance $S_{22}$ and modulus $Q_{22}$

$$S_{22}(t)/S_{22}(0) = g_o - \sum_{i=1}^{N} g_i \exp\left(- t/\lambda_i\right)$$

$$Q_{22}(t)/Q_{22}(0) = f_o + \sum_{i=1}^{N} f_i \exp\left(- t/\lambda_i\right)$$

| i | $g_i$ | $f_i$ | $\lambda_i$ |
|---|-------|-------|-------------|
| 0 | 2.15423 | 0.46420 | |
| 1 | 0.37010 | 0.07427 | $1.7280 \times 10^5$ |
| 2 | 0.39842 | 0.12371 | $3.1572 \times 10^4$ |
| 3 | 0.27249 | 0.22633 | $5.0198 \times 10^3$ |
| 4 | 0.06688 | 0.06466 | $6.110 \times 10^2$ |
| 5 | 0.04634 | 0.04683 | $1.007 \times 10^2$ |

50.8 mm

Grating

Dia. 6.35 mm

Tab

50.8 mm

254 mm
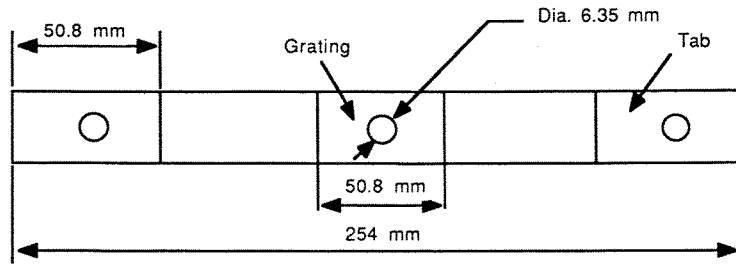
a) Specimen geometry and dimensions

y

Strain Gage #2

9.5 mm

25.4 mm

a

$\phi$
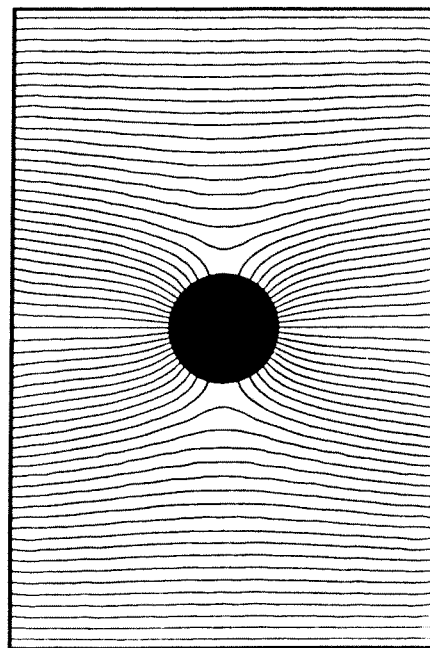
x

5.7 mm
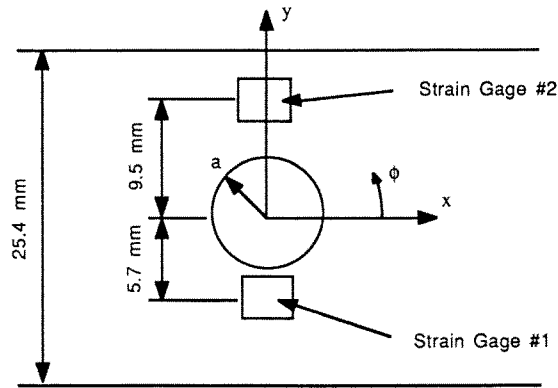
Strain Gage #1

b) Strain gage locations

Fig. 1 Configuration of specimen
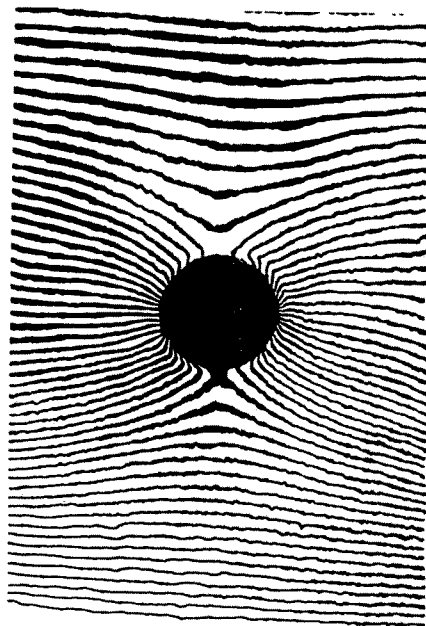
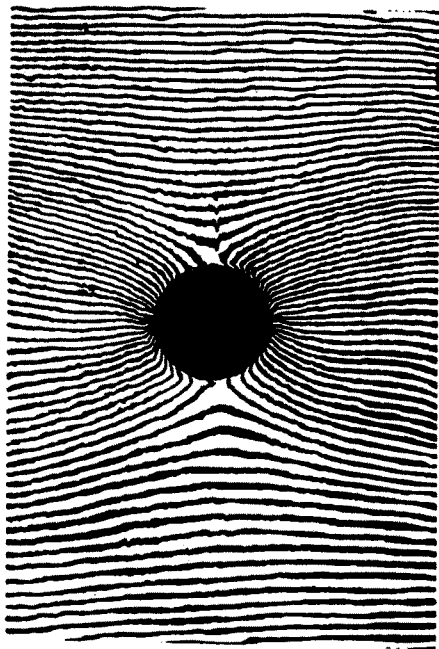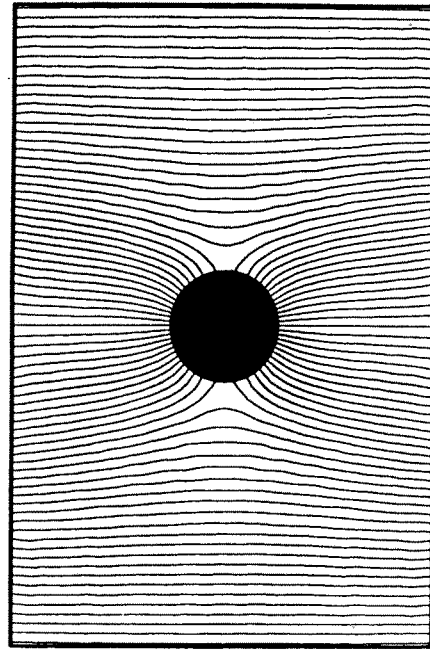

a) Moire fringe pattern

b) Contour from finite element analysis

Fig. 2 Comparison of axial displacements in a $(90_2/\pm45/90/\pm45/90)_s$ laminate, $121°$ C, t = 1 min.

a) Moire fringe pattern



b) Contour from finite element analysis

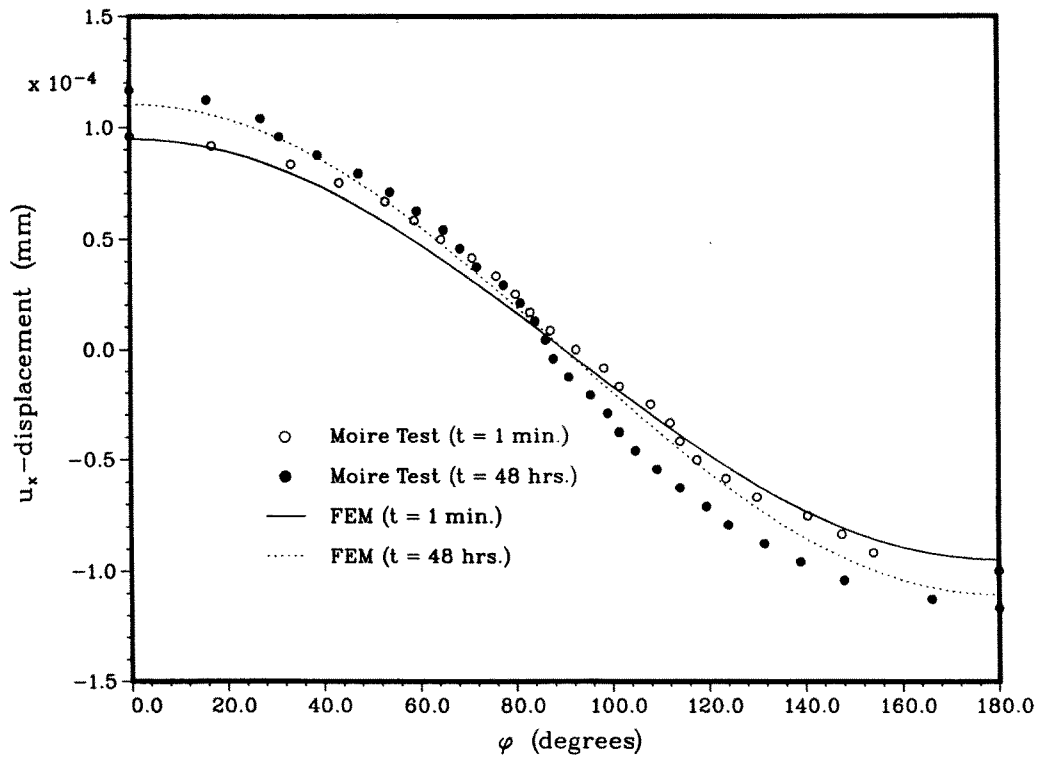Fig. 3 Comparison of axial displacements in a $(90_2/\pm45/90/\pm45/90)_s$ laminate, 121° C, t = 48 hrs.



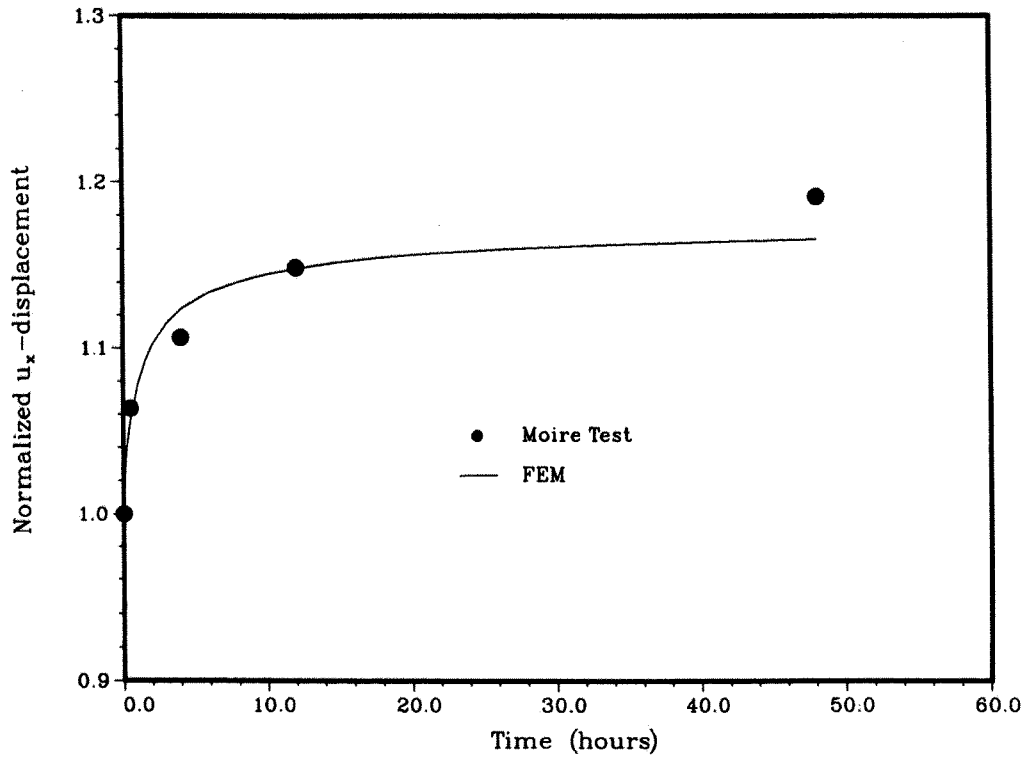Fig. 4 Displacement distributions along the hole edge of a $(90_2/\pm45/90/\pm45/90)_s$ laminate

Fig. 5 Time-dependent displacement in a $(90_2/\pm45/90/\pm45/90)_s$ laminate, $121°$ C
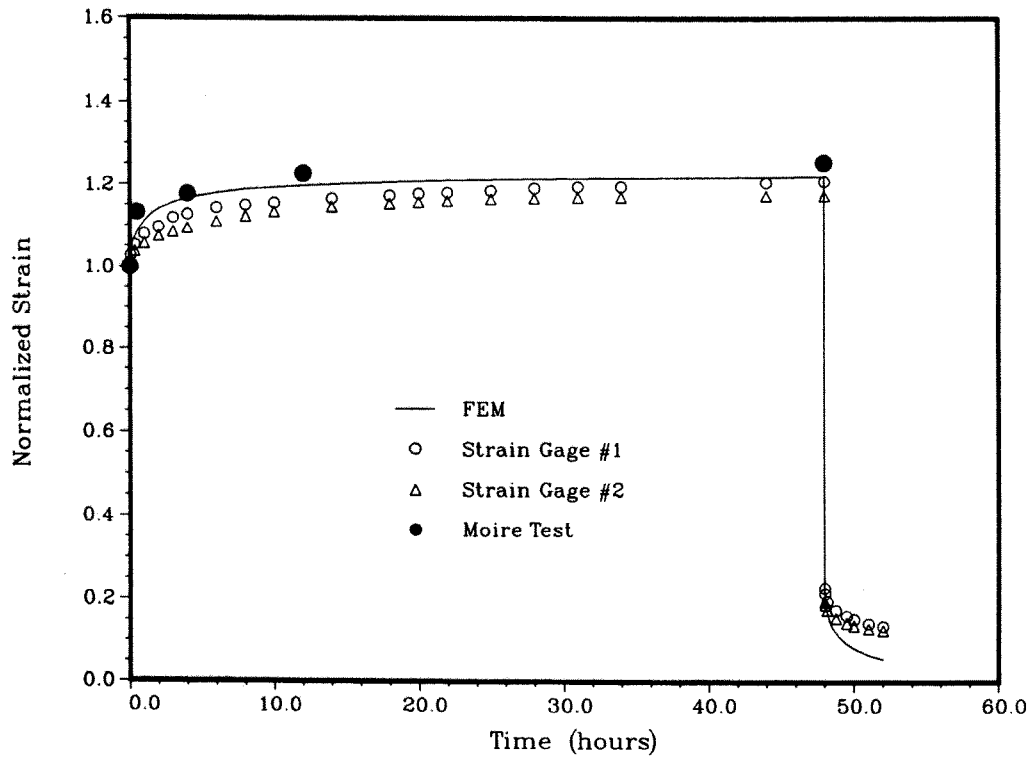


Fig. 6 Comparison of strains in a $(90_2/\pm45/90/\pm45/90)_s$ laminate